EUROPHYSICS LETTERS

OFFPRINT

Vol. 71 • Number 2 • pp. 283–289

Transport property in $SrTiO_3$ p-n junction

* * *

Qing-li Zhou, Kui-juan Jin, Hui-bin Lu, Peng Han, Zheng-hao Chen,
Kun Zhao, Yue-liang Zhou and Guo-zhen Yang

Published under the scientific responsability of the
EUROPEAN PHYSICAL SOCIETY
Incorporating
JOURNAL DE PHYSIQUE LETTRES • LETTERE AL NUOVO CIMENTO

EUROPHYSICS LETTERS

Editor-in-Chief

Prof. Denis Jérome
Lab. Physique des Solides - Université Paris-Sud
91405 Orsay - France
jerome@lps.u-psud.fr

Staff Editor: Yoanne Sobieski
Europhysics Letters, European Physical Society, 6 rue des Frères Lumière, 68200 Mulhouse, France

Editorial Director: Angela Oleandri
Production Editor: Paola Marangon
Director of publication: Jean-Marc Quilbé

Publishers: EDP Sciences S.A., France - Società Italiana di Fisica, Italy

Taking full advantage of the service on Internet, please choose the fastest connection:

http://www.edpsciences.org
http://edpsciences.nao.ac.jp
http://edpsciences-usa.org
http://www.epletters.ch

Europhysics Letter was launched more than fifteen years ago by the European Physical Society, the Société Française de Physique, the Società Italiana di Fisica and the Institute of Physics (UK) and owned now by 17 National Physical Societies/Institutes.

Europhysics Letters aims to publish short papers containing non-trivial new results, ideas, concepts, experimental methods, theoretical treatments, etc. which are of broad interest and importance to one or several sections of the physics community.

Europhysics letters provides a platform for scientists from all over the world to offer their results to an international readership.

Subscription 2005

24 issues - Vol. 69-72 (6 issues per vol.)

ISSN: 0295-5075 - ISSN electronic: 1286-4854

- France & EU (VAT included) ☐ 1 795 €
- Rest of the World (without VAT) ☐ 1 795 €

Payment:

❐ Check enclosed payable to EDP Sciences

❐ Please send me a pro forma invoice

❐ Credit card:

❐ Visa ❐ Mastercard ❐ American Express

Valid until: |_|_|_|_|

Card No: |_|_|_|_|_|_|_|_|_|_|_|_|_|_|_|_|

❐ Please send me a **free** sample copy

Institution/Library: ....

....

Name: ....

Position: ....

Address: ....

....

....

ZIP-Code: ....

City: ....

Country: ....

E-mail: ....

Signature:

Order through your subscription agency or directly from EDP Sciences:
17 av. du Hoggar • B.P. 112 • 91944 Les Ulis Cedex A • France
Tel. 33 (0)1 69 18 75 75 • Fax 33 (0)1 69 86 06 78 • subscribers@edpsciences.org

EUROPHYSICS LETTERS 15 July 2005

Europhys. Lett., **71** (2), pp. 283–289 (2005)
DOI: 10.1209/epl/i2005-10084-4

Transport property in $SrTiO_3$ *p*-*n* junction

Qing-li Zhou, Kui-juan Jin(*), Hui-bin Lu, Peng Han, Zheng-hao Chen, Kun Zhao, Yue-liang Zhou and Guo-zhen Yang

Beijing National Laboratory for Condensed Matter Physics, Institute of Physics Chinese Academy of Science - P.O. Box 603, Beijing 100080, PRC

received 18 March 2005; accepted in final form 26 May 2005
published online 17 June 2005

PACS. 73.40.Lq – Other semiconductor-to-semiconductor contacts, *p*-*n* junctions, and heterojunctions.
PACS. 77.84.Dy – Niobates, titanates, tantalates, PZT ceramics, etc.
PACS. 72.20.Dp – General theory, scattering mechanisms.

Abstract. – The transport properties of a homogenous perovskite oxide *p*-*n* junction composed of the *p*-type In-doped $SrTiO_3$ and *n*-type Nb-doped $SrTiO_3$ have been studied by solving one-dimensional steady-state carrier-transport equations based on the drift-diffusion model. The energy band profile, electric-field intensity, and charge density are obtained for the space charge region at various bias voltages. Furthermore, the rectifying characteristics of the *I*-*V* curves are calculated and analyzed as a function of doping density. The theoretical results are in good agreement with the experimental data, and more details in the understanding of transport mechanism for oxide *p*-*n* junctions have been gained.

Since the colossal magnetoresistance in manganitesthe was observed, much attention has been focused on the fabrication of all-oxide perovskite structures and devices, such as tunnel junctions [1] and *p*-*n* junctions [2,3]. Strontium titanate $SrTiO_3$ (STO) with a relative dielectric constant as high as 300 at room temperature (RT) [4,5] has been widely studied due to its variety of applications [6]. Stoichiometric STO with a simple-cubic perovskite structure (lattice constant $a = 0.3905\,\text{nm}$) is an insulator at RT with the band gap of $3.2\,\text{eV}$ [7,8], whereas its electrical properties can be changed by doping with impurity atoms [9–13]. In the study of thin-film growth, STO is very often used as the substrate for depositing other perovskite oxides owing to the small in-plane lattice mismatch [14]. With its notable dielectric and doped semiconducting properties, STO can be utilized to develop field effect device [15] besides the use in dynamic random-access memories, and high-density capacitors, etc. Furthermore, there are many reports with good results in the optoelectronic characteristics of bulk STO [16], optical property [6,17], resistivity characteristics, and surface spectroscopy studies [18] on the doped STO. However, few studies have been carried out on the transport properties of the homogenous *p*-*n* junction of STO. We utilized a computer-controlled laser molecular-beam epitaxy (laser MBE) [19] to homoepitaxially fabricate the all-perovskite oxide *p*-type In-doped and *n*-type Nb-doped STO junction. Moreover, the deposited $SrTi_{0.8}In_{0.2}O_3/SrTi_{0.99}Nb_{0.01}O_3$ (In-STO/Nb-STO) junction presents good *I*-*V* rectifying characteristics. To understand the

(*) E-mail: kjjin@aphy.iphy.ac.cn

© EDP Sciences

physics properties of this kind of oxide p-n junction further, theoretical study has been expected since computer-aided simulation is one of the important processes in developing semiconductor devices.

In this paper, on the basis of the drift-diffusion model, we obtained electrostatic potential, electron and hole concentrations by solving the coupled nonlinear differential equations of current continuity and Poisson equations self-consistently using Gauss-Seidel iteration [20]. Under the applied bias voltage, the I-V characteristics of p-n junction were obtained and compared with the experimental data. Finally, the changes of the I-V curves as a function of doping density were discussed theoretically.

For a semiconductor, the behavior of carriers under the external fields can be described by Poisson equation, electron and hole continuity equations on the basis of drift-diffusion theory [21]. For one-dimensional steady-state, the Poisson equation is expressed as follows:

$$\frac{\mathrm{d}^2\psi(x)}{\mathrm{d}x^2} = -\frac{q}{\varepsilon}[p(x) - n(x) + N], \tag{1}$$

where $\psi(x)$ denotes the electrostatic potential, q is the elementary charge, ε is the dielectric constant, $p(x)$ and $n(x)$ are the hole and electron carrier densities. The net impurity concentration N is equal to $-N_a$ (N_a is the acceptor impurity concentration) in the p-region and equal to $+N_d$ (N_d is the donor impurity concentration) in the n-region with assumption of complete ionization. The continuity equations for electrons and holes are given by

$$\frac{\mathrm{d}J_n}{\mathrm{d}x} = q[R(x) - G], \tag{2}$$

$$\frac{\mathrm{d}J_p}{\mathrm{d}x} = -q[R(x) - G], \tag{3}$$

where J_n and J_p are current densities for electrons and holes, respectively, which are given by the following equations:

$$J_n = -q\mu_n n(x)\frac{\mathrm{d}\psi(x)}{\mathrm{d}x} + k_B T\mu_n\frac{\mathrm{d}n(x)}{\mathrm{d}x}, \tag{4}$$

$$J_p = -q\mu_p p(x)\frac{\mathrm{d}\psi(x)}{\mathrm{d}x} - k_B T\mu_p\frac{\mathrm{d}p(x)}{\mathrm{d}x}, \tag{5}$$

where μ_n and μ_p are the electron and hole mobilities, the symbol k_B is Boltzmann's constant, and T is the temperature. In eqs. (2) and (3), $R(x)$ and G denote the recombination and generation rates and are assumed to be specified by the Shockley-Read-Hall model [22,23]:

$$[R(x) - G] = \frac{p(x)n(x) - n_i^2}{\tau_{n0}[p(x) + n_i] + \tau_{p0}[n(x) + n_i]}, \tag{6}$$

where n_i is the intrinsic carrier density, and τ_{n0} and τ_{p0} are the lifetime for electrons and holes, respectively. Furthermore, the total conduction current is expressed by $J = J_n + J_p$. The electric-field dependence of mobilities is not considered here for simplification.

The boundary conditions can be specified as charge density $\rho = 0$ far away from the space charge region of the p-n junction. The electrostatic potentials of the p and n side far away from the space charge region are set to be 0 and $V_d - V_{bias}$, respectively, where V_d is the built-in potential difference and V_{bias} is the bias voltage. The Gauss-Seidel method is used to solve eqs. (1)-(3) iteratively with the primal state variables $(\psi(x), p(x), n(x))$. In the iteration, the energy band profiles and the electron and hole concentrations are updated by solving those three equations self-consistently.

TABLE I – *Material parameters used in the calculation.*

Parameter	Value
Temperature (K)	$T = 300$
Band gap (eV)	$E_g = 3.2$
Electron effective mass (m_0)	$m_n^* = 16$
Hole effective mass (m_0)	$m_p^* = 16$
Dielectric constant (ε_0)	$\varepsilon = 150$
Electron lifetime (s)	$\tau_{n0} = 10^{-9}$
Hole lifetime (s)	$\tau_{p0} = 10^{-9}$

The model described in the above section is applied to the In-STO/Nb-STO junction. To fabricate this junction, laser MBE [19] was used to deposit In-STO directly on 1% Nb-doped STO substrate. The substrate temperature was kept at 610 °C under 3×10^{-4} Pa oxygen pressure. The thickness of In-STO thin film is about 500 nm. Then the film was annealed for 30 minutes under the oxygen pressure of $\sim 1 \times 10^{-2}$ Pa. During the deposition, an *in situ* reflection high-energy electron diffraction (RHEED) was used to monitor the growth process. The good RHEED pattern indicats the film had high crystallinity. The sample was characterized with X-ray diffraction (XRD), showing the film was of single phase. Through the X-ray photoemission spectroscopy (XPS) and Hall measurement, Dai *et al.* [13] found In-ions in the In-STO film were in the 3+ valence state and the charge carriers were *p*-type, showing the In content is implemented on the B-site. The carrier mobility of the *p*-type In-STO film is about 6 cm^2/Vs. The mobility of the *n*-type Nb-STO is about 8 cm^2/Vs obtained in ref. [16] as the

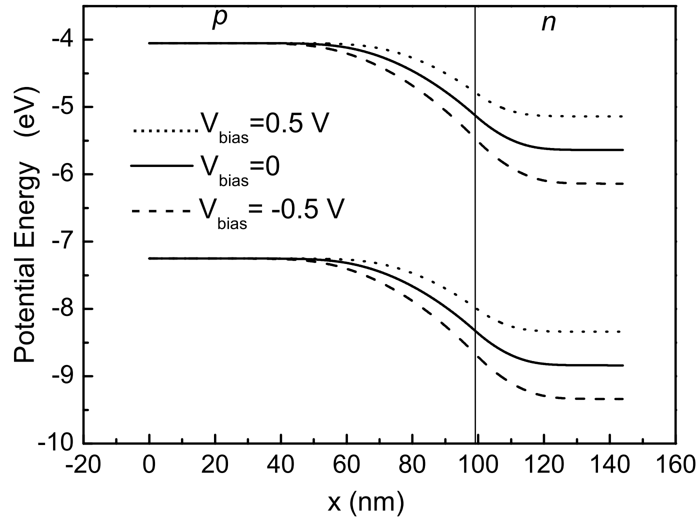

Fig. 1 – Energy-band diagrams under the positive and reverse bias voltages. The vertical solid line represents the interface of the *p-n* junction. The solid, dotted and dashed lines correspond to $V_{bias} = 0$ V, 0.5 V, −0.5 V, respectively.

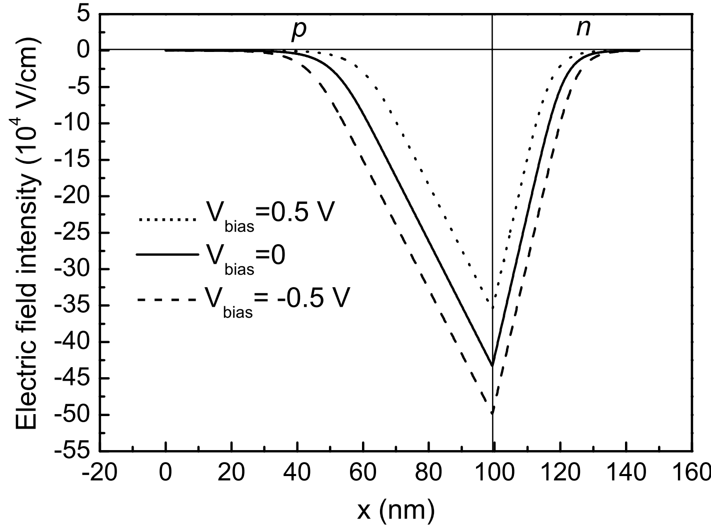

Fig. 2 – Distributions of electric-field intensity in space at various applied bias voltages. The solid, dotted and dashed lines correspond to $V_{bias} = 0\,\text{V}$, $0.5\,\text{V}$, $-0.5\,\text{V}$, respectively.

parameter for simplification, which is consistent with the result in Moos's paper [24]. Chambers *et al.* [25] have reported that the conduction band offsets are $0.1 \pm 0.1\,\text{eV}$ and $0.0 \pm 0.1\,\text{eV}$ for STO on n-Si and STO on p-Si, respectively. So we simply assume that the conduction band offset between STO and Si is zero, then obtain the affinity energy of STO is about 4.05 eV, equal to that of Si material. Other material parameters utilized in the present work are listed in table I [7, 26, 27]. To determine the electrical behaviors, the sample was cut into $2 \times 2\,\text{mm}^2$ for the electrical measurements. And the current-voltage curve will be shown later.

The potential energy diagrams showing the effect of various bias voltages upon the energy band configuration at a p-n junction are shown in fig. 1, with the parameters of $N_a = 7.34 \times 10^{18}\,\text{cm}^{-3}$ and $N_d = 1.63 \times 10^{19}\,\text{cm}^{-3}$. When an external low voltage is applied to the junction, the voltage dropping across the uniform n- and p-regions outside the space charge region is negligible in comparison with the drop across the junction region itself. The solid, dotted and dashed lines denote the shapes of the energy bands under the zero (0 V), positive (0.5 V) and reverse (−0.5 V) bias, respectively. It can be seen from fig. 1 that the positive bias reduces the potential barrier and the negative bias increases the potential barrier.

Accordingly, the distributions of electric-field intensity under various applied voltages are given in fig. 2. Under the positive bias, the values of the electric-field intensity are smaller than those without bias. Contrariwise, under the reverse bias, the values of the electric field intensity become larger than those without bias. The charge density reaches a constant of $-qN_a$ close to the interface in the p side and reaches a constant of qN_d close to the interface in the n side, as shown in fig. 3. Furthermore, with the application of the bias voltage, the space charge region will shrink or enlarge according to the positive or negative voltage, as shown by the dotted line (0.5 V) or dashed line (−0.5 V).

In practical simulation, the current *vs.* voltage curves of the device are usually of interest,

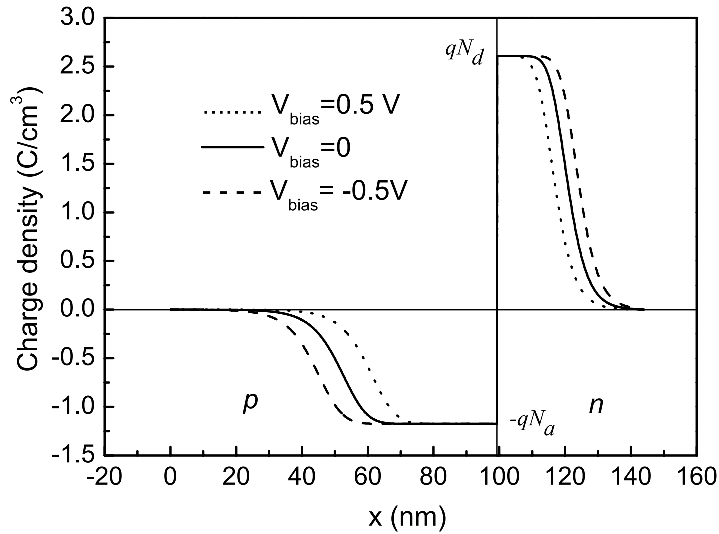

Fig. 3 – Distributions of charge density in space at various applied bias voltages. The solid, dotted and dashed lines correspond to $V_{bias} = 0\,\text{V}$, $0.5\,\text{V}$, $-0.5\,\text{V}$, respectively.

so the *I-V* characteristics are analyzed in the present paper. The theoretical and experimental *I-V* curves of the *p-n* junction at the temperature $T = 300\,\text{K}$ are shown in fig. 4. The full circles and triangles represent the theoretical and experimental results, respectively. Study of *I-V* characteristics of the theoretical results shows a stronger asymmetry in the positive and reverse bias voltages than that in the experiment. This feature is due to the neglect of the leakage current in our calculation. The difference between the theoretical and experimental curves may be attributed to many reasons, such as the neglect of the leakage current, the approximation of the material parameters' values, and the growth condition during the *p-n* junction's fabrication which induces the parameters of sample slightly deviate from references.

The studies on the effects of the doping density also have demonstrated that the junction displays the rectifying characteristics, as shown in fig. 5. Comparing the theoretical *I-V* curves for three different doping densities of N_a, it is easy to find that the main difference between those three curves is the current value under the large positive bias voltage. For instance, when the applied voltage is $1.0\,\text{V}$, the current is $6.04\,\text{mA}$ for $N_a = 7.34 \times 10^{18}\,\text{cm}^{-3}$ (open squares), but decreases to $4.34\,\text{mA}$ for N_a falling to $2.0 \times 10^{18}\,\text{cm}^{-3}$ (open triangles) and increases to $6.85\,\text{mA}$ for N_a rising to $7.34 \times 10^{19}\,\text{cm}^{-3}$ (open circles). With the increasing of the doping density with indium, the value of the current across the junction goes up owing to the reduction of resistivity originating from the enhancement of the carrier concentration [5]. The theoretical results are identical with the experimental measurement [3].

In summary, a theoretical model based on the drift-diffusion theory is presented to obtain the current *vs.* voltage characteristics of the In-STO/Nb-STO *p-n* junction by solving the coupled nonlinear differential equations. The distributions of potential energy, electric-field intensity, and charge density have been obtained at various bias voltages near the interface region. In addition, the *I-V* curves are obtained and analyzed as a function of the doping

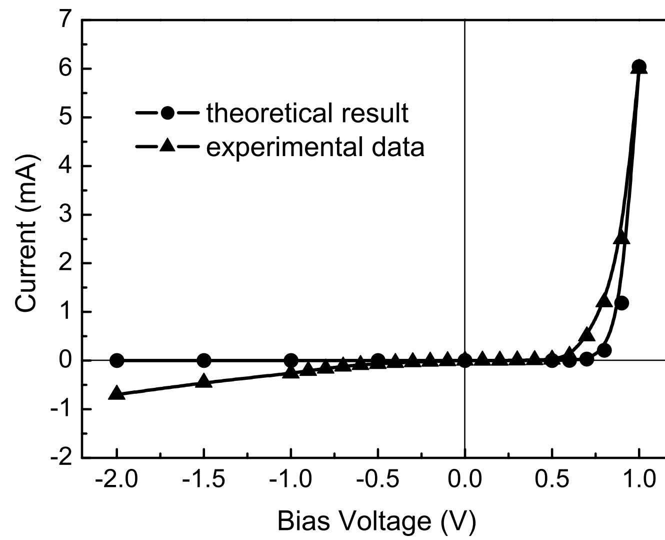

Fig. 4 – Theoretical I-V curve (full circles) compared with the experimental data (full triangles).

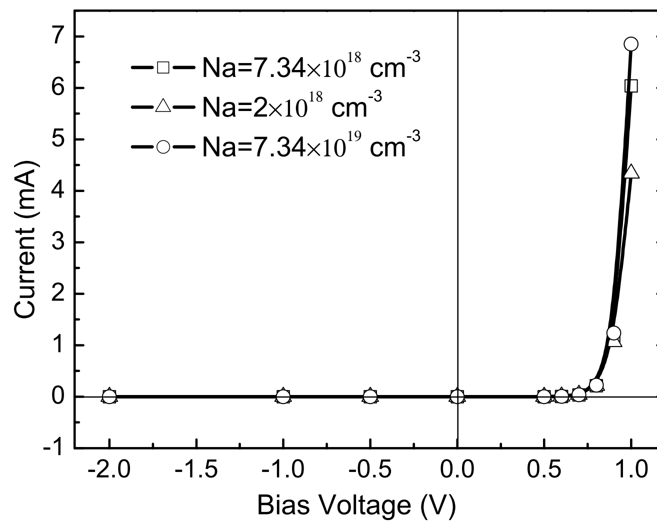

Fig. 5 – Calculated results of I-V curves for the STO p-n junction at the different doping densities of N_a. Open squares, triangles and circles correspond to $N_a = 7.34 \times 10^{18}\,\mathrm{cm}^{-3}$, $2 \times 10^{18}\,\mathrm{cm}^{-3}$, $7.34 \times 10^{19}\,\mathrm{cm}^{-3}$, respectively.

density. The agreement between theoretical and experimental results obtained in the junction indicates that the present model can be used as a tool to study and simulate the perovskite oxide semiconductor devices.

* * *

We gratefully acknowledge the financial support from the National Natural Science Foundation of China.

REFERENCES

[1] LU Y., LI X. W., GONG G. Q. *et al.*, *Phys. Rev. B*, **54** (1996) R8357.
[2] LU H. B., YANG G. Z., CHEN Z. H. *et al.*, *Appl. Phys. Lett.*, **84** (2004) 5007.
[3] LU H. B., DAI S. Y., CHEN Z. H. *et al.*, *Appl. Phys. Lett.*, **86** (2005) 032502.
[4] NEVILLE R. C., HOENEISEN B. and MEAD C. A., *J. Appl. Phys.*, **43** (1972) 2124.
[5] TOMIO T., MIKI H., TABATA H. *et al.*, *J. Appl. Phys.*, **76** (1994) 5886.
[6] GUO X. G., CHEN X. S. and LU W., *Solid State Commun.*, **126** (2003) 441.
[7] CARDONA M., *Phys. Rev.*, **140** (1965) A651.
[8] LO W. J. and SOMORJAI G. A., *Phys. Rev. B*, **17** (1978) 4942.
[9] REIHL B., BEDNORZ J. G., MÜLLER K. A. *et al.*, *Phys. Rev. B*, **30** (1984) 803.
[10] KOHIKI S., ARAI M., YOSHIKAWA H. *et al.*, *Phys. Rev. B*, **62** (2000) 7964.
[11] YUAN G. L., LIU J.-M., BABA-KISHI K. *et al.*, *Solid State Commun.*, **131** (2004) 383.
[12] HIGUCHI T., TSUKAMOTO T., SATA N. *et al.*, *Phys. Rev. B*, **57** (1998) 6978.
[13] DAI S., LU H., CHEN F. *et al.*, *Appl. Phys. Lett.*, **80** (2002) 3545.
[14] VIGLIANTE A., GEBHARDT U., RÜHM A. *et al.*, *Europhys. Lett.*, **54** (2001) 619.
[15] BELLINGERI E., PELLEGRINO L., MARRÉ D. *et al.*, *J. Appl. Phys.*, **94** (2003) 5976.
[16] MYHAJLENKO S., BELL A., PONCE F. *et al.*, *J. Appl. Phys.*, **97** (2005) 014101.
[17] GUO H., LIU L., FEI Y. *et al.*, *J. Appl. Phys.*, **94** (2003) 4558.
[18] CHUNG YIP-WAH and WEISSBARD W. B., *Phys. Rev. B*, **20** (1979) 3456.
[19] YANG G. Z., LU H. B., CHEN F. *et al.*, *J. Crystal Growth*, **227-228** (2001) 929.
[20] BARRETT R. *et al.*, *Templates for the Solution of Linear Systems: Building Blocks for Iterative Methods* (SIAM, Philadelphia) 1994.
[21] SZE S. M., *Physics of Semiconductor Devices* (Wiley, New York) 1981.
[22] YANG K., EAST J. R. and HADDAD G. I., *Solid State Electr.*, **36** (1993) 321.
[23] HORIO K., IWATSU Y. and YANAL H., *IEEE Trans. Electron Devices*, **36** (1989) 617.
[24] MOOS R. and HÄRDTL K. H., *J. Appl. Phys.*, **80** (1996) 393.
[25] CHAMBERS S. A., LIANG Y., YU Z. *et al.*, *Appl. Phys. Lett.*, **77** (2000) 1662.
[26] FREDERIKSE H. P. R., THURBER W. R. and HOSLER W. R., *Phys. Rev.*, **134** (1964) A442.
[27] HÖLBLING T. and WASER R., *J. Appl. Phys.*, **91** (2002) 3037.